Journal of Advanced Marine Engineering and Technology, Vol. 47, No. 5, pp. 226~230, 2023
J. Advanced Marine Engineering and Technology (JAMET)
https://doi.org/10.5916/jamet.2023.47.5.226

ISSN 2234-7925 (Print)
ISSN 2765-4796 (Online)
Original Paper

Effect of metal ratios on oxygen evolution reaction activity in binary hydroxide electrocatalysts

Seo Hyun Park[1] · Yoo Sei Park[†]

(Received August 26, 2023 ; Revised September 6, 2023 ; Accepted September 18, 2023)

Abstract: Electrochemical water splitting is a promising technology to produce hydrogen energy from water utilizing electricity. However, the sluggish kinetics of an oxygen evolution reaction (OER) hinder the achievement of high energy efficiency, acting as a barrier to the widespread adoption of electrolysis technology. Herein, we have developed $Cu_xCo_y(OH)_2$ by incorporating Cu into $Co(OH)_2$. Furthermore, we systematically analyzed the structural and electrochemical characteristics based on the ratio of Cu to Co. Despite incorporating Cu into $Co(OH)_2$, the nanosheet shape was relatively well-preserved. Nevertheless, an excessive Cu content in $Cu_xCo_y(OH)_2$ led to the transformation of nanosheets into polygonal shapes. Increasing Cu content improved OER activity, but excessive Cu diminished OER activity, resulting in changes in surface shape and crystal structure. This study highlights the significance of compositional optimization in developing binary hydroxide-based OER electrocatalysts.

Keywords: Hydrogen, Oxygen evolution reaction, Water splitting, Electrocatalysis, Water electrolysis

1. Introduction

Water electrolysis is a sustainable and eco-friendly technology that enables large-scale green hydrogen production without carbon emission. This process involves two half-reactions: an oxygen evolution reaction (OER, $4OH^- \rightarrow O_2 + 2H_2O + 4e^-$) and a hydrogen evolution (HER, $2H_2O + 2e^- \rightarrow 2OH^- + H_2$). While the HER directly contributes to hydrogen production, the OER primarily determines the overall efficiency of water electrolysis. The intrinsic sluggish kinetics of OER causes a large overpotential for water electrolysis, resulting in low energy efficiency. Therefore, a highly active electrocatalyst for OER is required to achieve high-efficiency water electrolysis.

Precious metal-based electrocatalysts such as RuO_2 and IrO_2 are considered the best OER electrocatalysts owing to their high catalytic activity for OER. However, their usage is limited because of their high cost and scarcity. To address these challenges, a wide variety of non-precious metal-based electrocatalysts have been developed, such as transition metal oxide **[6][8][17]**, transition metal phosphide **[12][21]**, transition metal sulfide **[14]**, and transition metal hydroxide **[2][4][9][22]**. Among them, transition metal hydroxides have demonstrated significant promise as low-cost and active OER electrocatalysts because they can be synthesized at low temperatures while delivering high performance. Among various hydroxides, $Ni(OH)_2$ and $Co(OH)_2$ have been identified to possess good OER activity **[4][13]**. However, their OER activity is relatively poor compared to precious metal-based electrocatalysts. A modification of the electronic structure is necessary to enhance the catalytic activity for OER, which can be achieved by introducing a second metal element. Cu, in particular, is known for its excellent electron conductivity and exists in two oxidation states, +1 and +2, making it a suitable element to modify the electronic structure of $Ni(OH)_2$ or $Co(OH)_2$.

So far, transition metal hydroxides have been synthesized through various methods, such as hydrothermal methods **[3]**, co-precipitation **[5]**, corrosion engineering **[11][20]**, and electrodeposition **[15][16]**. Among these methods, electrodeposition offers distinct benefits compared to other processes. This process can be performed at room temperature, is simple, and requires a short time for synthesizing the transition metal hydroxide. Moreover, by controlling the potential, time, and composition of dissolved metal salts in the electrodeposition solution, a different nanostructure can be obtained **[7][19]**.

† Corresponding Author (ORCID: http://orcid.org/0000-0002-5154-2323): Assistant Professor, Department of Advanced Material Engineering, Chungbuk National University, Chungdae-ro 1, Seowon-Gu, Cheongju, Chungbuk 28644, Republic of Korea, E-mail: yspark@chungbuk.ac.kr, Tel: +82-43-261-2418

1 Undergraduate Student, Department of Advanced Material Engineering, Chungbuk National University, E-mail: seohyeon.p01@gmail.com

Here, we systematically investigated the effect of the ratio of Cu and Co in $Cu_xCo_y(OH)_2$ for OER. $Co(OH)_2$ without Cu exhibited a nanosheet shape, and $Cu_xCo_y(OH)_2$ with an appropriate amount of Cu introduced well-maintained nanosheet shape. Furthermore, as the amount of Cu increased, it enhanced OER activity. However, excessive Cu introduction completely altered the surface shape, accompanied by a decline in the OER activity. This study highlights the significance of compositional optimization in developing binary hydroxide-based OER electrocatalysts.

2. Experiment

2.1 Preparation of $Cu_xCo_y(OH)_2$

$Cu_xCo_y(OH)_2$ was prepared on nickel foam (NF) through electrodeposition. To systematically analyze the effect of the composition of Cu and Co in $Cu_xCo_y(OH)_2$, the ratio of Cu^{2+} ion and Co^{2+} ion in the solution for electrodeposition was controlled (Cu^{2+}:Co^{2+} = 0:2, 0.2:0.8, 0.4:0.6, and 0.8/0.2). Before electrodeposition, NF was etched in 5 M HCl for 15 min to remove the surface oxide layer and then rinsed with deionized water (DI water). The metal ion concentration in the solution for electrodeposition was 50 mmol, where $Cu(NO_3)_2{\cdot}6H_2O$, $Co(NO_3)_2{\cdot}6H_2O$, and DI water (50 mL) were mixed under magnetic stirring for 30 min at 25 ℃. NF was adopted as a working electrode, and a titanium-felt was utilized as a counter electrode. A reference electrode was a saturated calomel electrode (SCE). The electrodeposition was carried out at 25 ℃ for 5 min by applying a constant potential of -1 V. Subsequently, the electrodeposited NF was rinsed with DI water and then dried in an oven.

2.2 Materials Characterization

The surface morphologies of $Cu_xCo_y(OH)_2$ were observed by field emission scanning electron microscopy (FE-SEM, CZ/MIRAI LMH, TESCAN). The crystal structure of $Cu_xCo_y(OH)_2$ was characterized by Cu Kα radiation in the range of 10−80° (2θ) utilizing X-ray diffraction (XRD, UltimaIV, Rigaku).

2.3 Electrochemical Characterization

All electrochemical measurements were performed in a three-electrode system under a 1.0-M KOH solution. The $Cu_xCo_y(OH)_2$ was employed as the working electrode, and a graphite rod was utilized as a counter electrode. A Hg/HgO (1 M KOH) electrode was adopted as the reference electrode. Linear sweep voltammetry was performed at a scan rate of 1 mV s^{-1} to obtain polarization curves, and 100% iR was corrected. The measured potential was calculated utilizing the Nernst equation: $E_{RHE} = E_{Hg/HgO} + 0.0591 \times pH + 0.098$. Electrochemical impedance spectroscopy was performed at a potential of 1.88 V (vs. RHE) from 10 kHz to 1 Hz. Durability was tested at a current density of 100 mA cm^{-1} for 180 h.

3. Results and Discussion

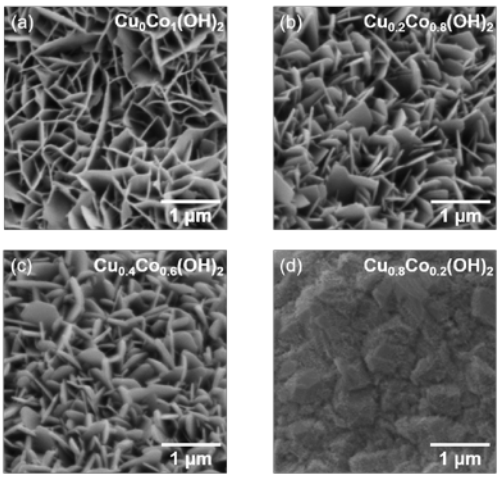

Figure 1: SEM images of (a) $Cu_0Co_1(OH)_2$, (b) $Cu_{0.2}Co_{0.8}(OH)_2$, (c) $Cu_{0.4}Co_{0.6}(OH)_2$, and (d) $Cu_{0.8}Co_{0.2}(OH)_2$

Table 1: Composition of $Cu_xCo_y(OH)_2$ by EDS analysis

Sample	Cu (at %)	Co (at %)
$Cu_0Co_1(OH)_2$	0	100
$Cu_{0.2}Co_{0.8}(OH)_2$	73	27
$Cu_{0.4}Co_{0.6}(OH)_2$	82	18
$Cu_{0.8}Co_{0.2}(OH)_2$	85	15

The surface morphologies of $Cu_xCo_y(OH)_2$ are presented in **Figure 1**. $Cu_0Co_1(OH)_2$ exhibited a nanosheet shape, and similar nanosheet shapes were observed for $Cu_{0.2}Co_{0.8}(OH)_2$ and $Cu_{0.4}Co_{0.6}(OH)_2$. However, noticeable differences were observed owing to the varying Cu content. As the Cu ratio increased, the nanosheets became thicker and transformed into polygonal shapes. Interestingly, the surface of $Cu_{0.8}Co_{0.2}(OH)_2$ differed significantly from the others, taking the form of particles rather than nanosheets **[18]**. EDS mapping images of $Cu_0Co_1(OH)_2$, $Cu_{0.2}Co_{0.8}(OH)_2$, $Cu_{0.4}Co_{0.6}(OH)_2$, and $Cu_{0.8}Co_{0.2}(OH)_2$ are presented in Figure 2a–d. These images enabled us to analyze the element distribution, and the results confirmed the uniform distribution of Cu, Co, and O in all four samples. Furthermore, EDS analysis revealed a clear correlation between the increasing

concentration of dissolved Cu^{2+} ion in the electrodeposition solution and a corresponding rise in the Cu content within $Cu_xCo_y(OH)_2$ (**Table 1**).

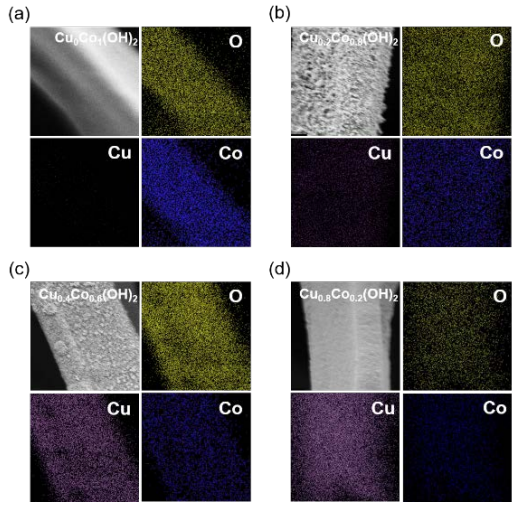

Figure 2: EDS mapping images of (a) $Cu_0Co_1(OH)_2$, (b) $Cu_{0.2}Co_{0.8}(OH)_2$, (c) $Cu_{0.4}Co_{0.6}(OH)_2$, and (d) $Cu_{0.8}Co_{0.2}(OH)_2$

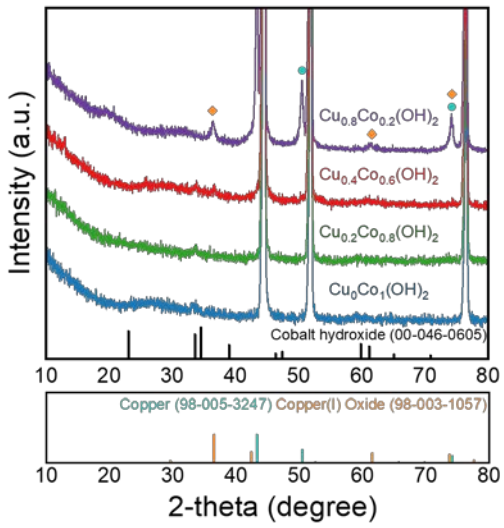

Figure 3: XRD patterns of $Cu_0Co_5(OH)_2$, $Cu_1Co_4(OH)_2$, $Cu_2Co_3(OH)_2$, and $Cu_4Co_1(OH)_2$

Remarkably, in all samples, the atomic percentage (at %) of Cu was higher than that of Co. This phenomenon can be attributed to the faster nucleation of Cu-based hydroxides compared to Co-based hydroxides during the initial stages of the electrodeposition process. As the electrodeposition process initiates, copper-based hydroxides form first, followed by the growth of $Cu_xCo_y(OH)_2$ on top of them. Consequently, the composition of all samples from the bulk catalyst layer exhibits a relatively higher quantity of Cu.

To investigate the crystal structure of $Cu_xCo_y(OH)_2$, X-ray diffraction (XRD) patterns were obtained and presented in **Figure 3**. The distinctive peaks at 44.5°, 51.8°, and 76.4° correspond to characteristic peaks of metallic nickel (JCPDS: 00-004-0850). Moreover, the cobalt hydroxide phase ($Co(OH)_2$, JCPDS: 00-046-0605) was observed in $Cu_0Co_1(OH)_2$, $Cu_{0.2}Co_{0.8}(OH)_2$, $Cu_{0.4}Co_{0.6}(OH)_2$, and $Cu_{0.8}Co_{0.2}(OH)_2$. Notably, in the XRD pattern of $Cu_{0.8}Co_{0.2}(OH)_2$, additional peaks were observed besides $Co(OH)_2$, which were indexed to copper(I) oxide (JCPDS: 98-003-1057) and metallic copper (JCPDS: 98-005-3247). Cu_2O was electrochemically precipitated owing to an excess of copper ions in the electrodeposition solution, and metallic Cu was deposited while continuously exposed to a reduction current **[18]**.

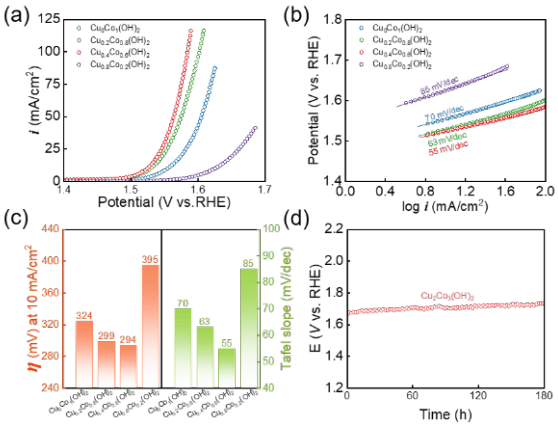

Figure 4: (a) Polarization curves of $Co(OH)_2$ and $Cu_xCo_{5-x}(OH)_2$ for OER. (b) Tafel plots of $Co(OH)_2$ and $Cu_xCo_{5-x}(OH)_2$. (c) Comparison of overpotential at 10 mA cm^{-2} and Tafel slopes of $Co(OH)_2$ and $Cu_xCo_{5-x}(OH)_2$. (d) Durability test of $Cu_{0.4}Co_{0.6}(OH)_2$ at 100 mA cm^{-2} for 180 h

The electrocatalytic activity of $Cu_xCo_y(OH)_2$ for OER was evaluated in a three-electrode system utilizing a 1.0-M KOH electrolyte, as illustrated in **Figure 4(a)**. The overpotential (η) required to achieve a current density of 10 mA/cm^2 was compared to assess the catalytic activity. The overpotential of $Cu_0Co_1(OH)_2$ was measured at 324 mV. The OER activity was improved as the amount of copper in $Cu_xCo_y(OH)_2$ increased. The overpotential of $Cu_{0.2}Co_{0.8}(OH)_2$ and $Cu_{0.4}Co_{0.6}(OH)_2$ was 299 mV and 293 mV, respectively, which were 25 mV and 31 mV lower than that of $Cu_0Co_1(OH)_2$. However, an excessive Cu content in $Cu_0Co_1(OH)_2$ led to an unexpected rise in the overpotential. This observation can be attributed to the significant presence of Cu_2O rather than the active Co-based hydroxide species. As Cu_2O exhibits poor OER activity compared to Co-based

hydroxides, its presence contributed to the increased overpotential **[10][23]**.

To gain deeper insights into the OER, we investigated the Tafel slopes derived from the polarization curves, as illustrated in **Figure 4(b)**. The Tafel slope represents the rate-determining step (RDS) in the OER, with smaller values indicating faster reaction kinetics. The Tafel slope of $Cu_0Co_1(OH)_2$ was calculated to be 70 mV dec^{-1}. Interestingly, the introduction of Cu reduced the value of the Tafel slope. $Cu_{0.2}Co_{0.8}(OH)_2$ and $Cu_{0.4}Co_{0.6}(OH)_2$ exhibited Tafel slopes of 63 mV dec^{-1} and 55 mV dec^{-1}, respectively, indicating that the introduction of Cu into $Co(OH)_2$ enhance the OER kinetics **[1]**. However, $Cu_{0.8}Co_{0.2}(OH)_2$ demonstrated a Tafel slope of 85 mV dec^{-1}, which is 15 mV dec^{-1} higher than that of $Cu_0Co_1(OH)_2$, indicating that the introduction of excess copper rather reduces the OER kinetics. The overpotentials and Tafel slopes for the samples were summarized in **Figure 4(c)**. Durability of $Cu_{0.4}Co_{0.6}(OH)_2$ test was performed at 100 mA/cm^2 for 180 h, as illustrated in **Figure 4(d)**. There was no significant change for 180 h, indicating good durability for OER.

4. Conclusion

This study investigated the changes in surface morphology and catalytic activity for OER based on the ratio of Cu and Co in $Cu_xCo_y(OH)_2$. Even with the introduction of Cu into $Co(OH)_2$, the nanosheet shape was relatively well-preserved. However, an excessive Cu content in $Cu_xCo_y(OH)_2$ led to the transformation of nanosheets into polygonal shapes. XRD analysis confirmed that an excess of Cu^{2+} ions in the electrodeposition solution leads to the precipitation of Cu_2O. $Cu_xCo_y(OH)_2$ (x:y = 0.4:0.6) exhibited enhanced OER activity compared to $Cu_0Co_5(OH)_2$. However, $Cu_{0.8}Co_{0.2}(OH)_2$, where Cu_2O is present, demonstrated poor OER activity. This study demonstrates the significance of compositional optimization in developing binary hydroxide-based OER electrocatalysts.

Acknowledgement

This research was supported by Chungbuk National University Korea National University Development Project (2022).

Author Contributions

Seo Hyun Park conducted the experiments, analyzed the data, and led the manuscript writing. Yoo Sei Park developed the intellectual concept, and provided supervisory guidance on experiments, data interpretation, and manuscript refinement.

References

[1] L. Chen, H. Zhang, L. Chen, X. Wei, J. Shi, and M. He, “Facile synthesis of Cu doped cobalt hydroxide (Cu–$Co(OH)_2$) nano-sheets for efficient electrocatalytic oxygen evolution,” Journal of Materials Chemistry A, vol. 5, pp. 22568-22575, 2017.

[2] Y. Deng, Y. Lu, R. Dai, M. Xiang, Z. Zhang, X. Zhang, and *et al.*, “Designing hierarchical iron doped nickel-vanadium hydroxide microsphere as an efficient electrocatalyst for oxygen evolution reaction,” Journal of Colloid and Interface Science, vol. 627, pp. 215-223, 2022.

[3] F. Dionigi, T. Reier, Z. Pawolek, M. Gliech, and P. Strasser, “Design criteria, operating conditions, and nickel–iron hydroxide catalyst materials for selective seawater electrolysis,” ChemSusChem, vol. 9, no. 9, pp. 962-972, 2016.

[4] M. Gao, W. Sheng, Z. Zhuang, Q. Fang, S. Gu, J. Jiang, and Y. Yan, “Efficient water oxidation using nanostructured α-nickel-hydroxide as an electrocatalyst,” Journal of the American Chemical Society, vol. 136, no. 19, pp. 7077-7084, 2014.

[5] M. J. Jang, J. Yang, J. Lee, Y. S. Park, J. Jeong, S. M. Park, and *et al.*, “Superior performance and stability of anion exchange membrane water electrolysis: pH-controlled copper cobalt oxide nanoparticles for the oxygen evolution reaction,” Journal of Materials Chemistry A, vol. 8, pp. 4290-4299, 2020.

[6] J. Y. Jeong, Y. S. Park, J. Jeong, K. B. Lee, D. Kim, K. Y. Yoon, and *et al.*, “A $NiCo_2O_4$ electrocatalyst with a thin graphitic coating for the anion exchange membrane water electrolysis of wastewater,” Journal of Materials Chemistry A, vol. 10, pp. 25070-25077, 2022.

[7] J. Yang, H. -H. Kim, B. -S. Kim, and Y. Kim, “Effects of various anode materials on the corrosion resistance of calcareous films deposited with an oyster shell waste-recycled solution,” Journal of Advanced Marine Engineering and Technology, vol. 46, no. 6, pp. 330-334, 2022.

[8] I. T. Kim, S. H. Kim, J. S. Ha, T. H. Kim, J. Cho, G. D. Park, and *et al.*, “Oxygen deficient yolk–shell structured Co3O4 microspheres as an oxygen evolution reaction electrocatalyst for anion exchange membrane water electrolyzers,” Journal of Materials Chemistry A, vol. 11, pp. 16578-16585, 2023.

[9] S. J. Lee and Y. S. Park, “Effect of synthesis temperature on oxygen evolution reaction of cobalt-iron layered double

hydroxide," Journal of Advanced Marine Engineering and Technology, vol. 46, no. 6, pp. 326-329, 2022.

[10] X. Liu, S. Cui, Z. Sun, Y. Ren, X. Zhang, and P. Du, "Self-supported copper oxide electrocatalyst for water oxidation at low overpotential and confirmation of its robustness by cu k-edge x-ray absorption spectroscopy," The Journal of Physical Chemistry C, vol. 120, no. 2, pp. 831-840, 2016.

[11] Y. Liu, X. Liang, L. Gu, Y. Zhang, G. D. Li, X. Zou, and *et al.*, "Corrosion engineering towards efficient oxygen evolution electrodes with stable catalytic activity for over 6000 hours," Nature Communications, vol. 9, 2018.

[12] Y. Liu, N. Ran, R. Ge, J. Liu, W. Li, Y. Chen, and *et al.*, "Porous Mn-doped cobalt phosphide nanosheets as highly active electrocatalysts for oxygen evolution reaction," Chemical Engineering Journal, vol. 425, 2021.

[13] D. McAteer D, I. J. Godwin, Z. Ling, A. Harvey, L. He, C. S. Boland, and *et al.*, "Liquid exfoliated $Co(OH)_2$ nanosheets as low-cost, yet high-performance, catalysts for the oxygen evolution reaction," Advanced Energy Materials, vol. 8, no. 15, 2018.

[14] M. Moradi, F. Hasanvandian, A. Bahadoran, A. Shokri, S. Zerangnasrabad, and B. Kakavandi, "New high-entropy transition-metal sulfide nanoparticles for electrochemical oxygen evolution reaction," Electrochimica Acta, vol. 436, 2022.

[15] Y. S. Park, W. S. Choi, M. J. Jang, J. H. Lee, S. Park, H. Jin, *et al.*, "Three-dimensional dendritic Cu–Co–P electrode by one-step electrodeposition on a hydrogen bubble template for hydrogen evolution reaction," ACS Sustainable Chemistry & Engineering, vol. 7, no. 12, pp. 10734-10741, 2019.

[16] Y. S. Park, J. Yang, J. Lee, M. J. Jang, J. Jeong, W. S. Choi, *et al.*, "Superior performance of anion exchange membrane water electrolyzer: Ensemble of producing oxygen vacancies and controlling mass transfer resistance," Applied Catalysis B: Environmental, vol. 278, 2020.

[17] J. Qi, W. Zhang, R. Xiang, K. Liu, H. Y. Wang, M. Chen, *et al.*, "Porous nickel–iron oxide as a highly efficient electrocatalyst for oxygen evolution reaction," Advanced Science, vol. 2, no. 10, 2015.

[18] A. S. M. Sayem Rahman, M. A. Islam, K. M. Shoroword, "Electrodeposition and characterization of copper oxide thin films for solar cell applications," Procedia Engineering, vol. 105, pp. 679-685, 2015.

[19] M. Skompska and K. Zarębska, "Electrodeposition of ZnO nanorod arrays on transparent conducting substrates – a Review," Electrochimica Acta, vol. 127, pp. 467-488, 2014.

[20] L. Wu, L. Yu, F. Zhang, D. Wang, D. Luo D, S. Song, and *et al.*, "Facile synthesis of nanoparticle-stacked tungsten-doped nickel iron layered double hydroxide nanosheets for boosting oxygen evolution reaction," Journal of Materials Chemistry A, vol. 8, no. 16, pp. 8096-8103, 2020.

[21] X. Xiao, C. T. He, S. Zhao, J. Li, W. Lin, Z. Yuan, *et al.*, "A general approach to cobalt-based homobimetallic phosphide ultrathin nanosheets for highly efficient oxygen evolution in alkaline media," Energy & Environmental Science, vol. 10, pp. 893-899, 2017.

[22] J. Xie, X. Zhang, H. Zhang, J. Zhang, S. Li, R. Wang, *et al.*, "Intralayered Ostwald ripening to ultrathin nanomesh catalyst with robust oxygen-evolving performance," Advanced Materials, vol. 29, no. 10, 2017.

[23] H. Xu, J. X. Feng, Y. X. Tong, and G. -R. Li, "Cu_2O–Cu hybrid foams as high-performance electrocatalysts for oxygen evolution reaction in alkaline media," ACS Catalysis, vol. 7, no. 2, pp. 986-991, 2017.